

Chapter 2

A Projection-Based Approach to Spectrum Sharing

Awais Khawar, Ahmed Abdelhadi and T. Charles Clancy

Spectrum sharing is a new way forward to solve spectrum scarcity problem. In this chapter, we first propose a spatial approach for spectrum sharing between a MIMO radar and an LTE cellular system with multiple base stations (BS). The MIMO radar and LTE share multiple interference channels. We propose projecting the radar signal onto the null space of interference channel between the MIMO radar and LTE using our proposed interference-channel-selection algorithm, in order to have zero-interference from the MIMO radar. We select interference channel with the maximum null space and project the radar signal onto the null space of this channel. Our proposed spatial spectrum sharing algorithm is radar-centric such that it causes minimum loss in radar performance by carefully selecting the interference channel and at the same time protects the i^{th} LTE BS from the radar interference. Through our analytical and simulation results we show that the loss in the radar performance is less when the proposed interference-channel-selection algorithm is used to select the channel onto which radar signals are projected. Second, we address the problem of target detection by radars that project waveform onto the null space of interference channel in order to mitigate interference to cellular systems. We consider a multiple-input multiple-output (MIMO) radar and a MIMO cellular communication system with multiple base stations (BS). We consider two spectrum sharing scenarios. In the first scenario the degrees of freedom (DoF) available at the radar are not sufficient enough to simultaneously detect target and mitigate interference to multiple BSs. For this case, we select one BS among many BSs for waveform projection

The content in this chapter is reproduced with permission after some modifications (License number 3926160879020 and 3926160775881). For the original article please refer to: A. Khawar, A. Abdelhadi, C. Clancy, "Target detection performance of spectrum sharing MIMO radars", IEEE Sens. J. 15, 4928-4940 (2015) and A. Khawar, A. Abdelhadi, C. Clancy, "Spectrum sharing between S-band radar and LTE cellular system: A spatial approach", IEEE International Symposium on Dynamic Spectrum Access Networks (2014).

on the basis of guaranteeing minimum waveform degradation. For the second case, the radar has sufficient DoF to simultaneously detect target and mitigate interference to all BSs. We study target detection capabilities of null-space projected (NSP) waveform and compare it with the orthogonal waveform. We derive the generalized likelihood ratio test (GLRT) for target detection and derive detector statistic for NSP and orthogonal waveform. The target detection performance for both waveforms is studied theoretically and via Monte Carlo simulations.

This chapter is organized as follows. Section 2.1 discuss MIMO radar, target channel, orthogonal waveforms, interference channel, and our cellular system model. Moreover, it also discusses modeling and statistical assumptions. Section 2.2 discusses spectrum sharing between MIMO radar and cellular system and introduces sharing architecture and projection algorithms. Section 2.3 discusses target parameter estimation performance for spectrum sharing radars followed by numerical results. Section 2.4.3 presents the generalized likelihood ratio test (GLRT) for target detection and derives detector statistic for NSP and orthogonal waveform followed by numerical results. Section 2.5 concludes the chapter.

2.1 System Model

In this section, we introduce preliminaries of MIMO radar, point target in far-field, orthogonal waveforms, interference channel, and cellular system model. Moreover, we also discuss modeling and statistical assumptions along with RF environment assumptions used throughout the chapter.

2.1.1 Radar Model

The radar we consider in this chapter is a colocated MIMO radar with M transmit and receive antennas and is mounted on a ship. The colocated MIMO radar has antennas that have spacing on the order of half the wavelength. Another class of MIMO radar is widely spaced MIMO radar where elements are widely spaced which results in enhanced spatial diversity [1]. The colocated radar gives better spatial resolution and target parameter identification as compared to the widely-spaced radar [2].

2.1.2 Target Model/Channel

In this chapter, we consider a point target model which is defined for targets having a scatterer with infinitesimal spatial extent. This model is a good assumption and is widely used in radar theory for the case when radar elements are colocated and there exists a large distance between the radar array and the target as compared to

inter-element distance [3]. The signal reflected from a point target with unit radar cross-section (RCS) is mathematically represented by the Dirac delta function.

2.1.3 Signal Model

Let $\mathbf{x}(t)$ be the signal transmitted from the M -element MIMO radar array, defined as

$$\mathbf{x}(t) = [x_1(t)e^{j\omega_c t} \ x_2(t)e^{j\omega_c t} \ \dots \ x_M(t)e^{j\omega_c t}]^T \quad (2.1)$$

where $x_k(t)e^{j\omega_c t}$ is the baseband signal from the k^{th} transmit element, ω_c is the carrier angular frequency, $t \in [0, T_o]$, with T_o being the observation time. We define the transmit steering vector as

$$\mathbf{a}_T(\theta) \triangleq [e^{-j\omega_c \tau_{T_1}(\theta)} \ e^{-j\omega_c \tau_{T_2}(\theta)} \ \dots \ e^{-j\omega_c \tau_{T_M}(\theta)}]^T. \quad (2.2)$$

Then, the transmit-receive steering matrix can be written as

$$\mathbf{A}(\theta) \triangleq \mathbf{a}_R(\theta)\mathbf{a}_T^T(\theta). \quad (2.3)$$

Since, we are considering M transmit and receive elements, we define $\mathbf{a}(\theta) \triangleq \mathbf{a}_T(\theta) \triangleq \mathbf{a}_R(\theta)$. The signal received from a single point target, in far-field with constant radial velocity v_r , at an angle θ can be written as

$$\mathbf{y}(t) = \alpha e^{-j\omega_D t} \mathbf{A}(\theta) \mathbf{x}(t - \tau(t)) + \mathbf{n}(t) \quad (2.4)$$

where $\tau(t) = \tau_{T_k}(t) + \tau_{R_l}(t)$, denoting the sum of propagation delays between the target and the k^{th} transmit element and the l^{th} receive element, respectively; ω_D is the Doppler frequency shift, α represents the complex path loss including the propagation loss and the coefficient of reflection, and $\mathbf{n}(t)$ is the zero-mean complex Gaussian noise.

2.1.4 Modeling Assumptions

In order to keep the analysis tractable we have made the following assumptions about our signal model:

- The path loss α is assumed to be identical for all transmit and receive elements, due to the far-field assumption [4].
- The angle θ is the azimuth angle of the target.
- After compensating the range-Doppler parameters, we can simplify Eq. (2.4) as

$$\mathbf{y}(t) = \alpha \mathbf{A}(\theta) \mathbf{x}(t) + \mathbf{n}(t). \quad (2.5)$$

2.1.5 Statistical Assumptions

We make the following assumptions for our received signal model in Eq. (2.5):

- θ and α are deterministic unknown parameters representing the target's direction of arrival and the complex amplitude of the target, respectively.
- The noise vector $\mathbf{n}(t)$ is independent, zero-mean complex Gaussian with known covariance matrix $\mathbf{R}_n = \sigma_n^2 \mathbf{I}_M$, i.e., $\mathbf{n}(t) \sim \mathcal{N}^c(\mathbf{0}_M, \sigma_n^2 \mathbf{I}_M)$, where \mathcal{N}^c denotes the complex Gaussian distribution.
- With the above assumptions, the received signal model in Eq. (2.5) has independent complex Gaussian distribution, i.e.,

$$\mathbf{y}(t) \sim \mathcal{N}^c(\alpha \mathbf{A}(\theta) \mathbf{x}(t), \sigma_n^2 \mathbf{I}_M). \quad (2.6)$$

2.1.6 Orthogonal Waveforms

In this chapter, we consider orthogonal waveforms transmitted by MIMO radars, i.e.,

$$\mathbf{R}_x = \int_{T_o} \mathbf{x}(t) \mathbf{x}^H(t) dt = \mathbf{I}_M. \quad (2.7)$$

The transmission of orthogonal signals gives MIMO radar advantages in terms of digital beamforming at the transmitter in addition to receiver, improved angular resolution, extended array aperture in the form of virtual arrays, increased number of resolvable targets, lower sidelobes [5], and lower probability of intercept as compared to coherent waveforms [4].

2.1.7 Communication System

In this chapter, we consider a MIMO cellular system, with \mathcal{K} base stations, each equipped with N^{BS} transmit and receive antennas, with i^{th} BS supporting $\mathcal{L}_i^{\text{UE}}$ user equipment (UE). The UEs are also multi-antenna systems with N^{UE} transmit and receive antennas. If $\mathbf{s}_j^{\text{UE}}(t)$ is the signals transmitted by the j^{th} UE in the i^{th} cell, then the received signal at the i^{th} BS receiver can be written as

$$\mathbf{r}_i(t) = \sum_j \mathbf{H}_j^{N^{\text{BS}} \times N^{\text{UE}}} \mathbf{s}_j^{\text{UE}}(t) + \mathbf{w}(t) \quad 1 \leq j \leq \mathcal{L}_i^{\text{UE}} \quad (2.8)$$

where $\mathbf{w}(t)$ is the additive white Gaussian noise.

2.1.8 Interference Channel

In this section, we characterize the interference channel that exists between MIMO cellular base station and MIMO radar. In our chapter, we are considering \mathcal{K} cellular BSs that is why our model has \mathbf{H}_i , $i = 1, 2, \dots, \mathcal{K}$, interference channels, where the entries of \mathbf{H}_i are denoted by

$$\mathbf{H}_i = \begin{bmatrix} h_i^{(1,1)} & \dots & h_i^{(1,M)} \\ \vdots & \ddots & \vdots \\ h_i^{(N^{\text{BS}},1)} & \dots & h_i^{(N^{\text{BS}},M)} \end{bmatrix} \quad (N^{\text{BS}} \times M) \quad (2.9)$$

where $h_i^{(l,k)}$ denotes the channel coefficient from the k^{th} antenna element at the MIMO radar to the l^{th} antenna element at the i^{th} BS. We assume that elements of \mathbf{H}_i are independent, identically distributed (i.i.d.) and circularly symmetric complex Gaussian random variables with zero-mean and unit-variance, thus, having a i.i.d. Rayleigh distribution. A more thorough treatment of interference channel modeling between radar and cellular system, including two- and three-dimensional channel models, can be found in [6–9].

2.1.9 Cooperative RF Environment

In the wireless communications literature, it is usually assumed that the transmitter (mostly BS) has channel state information (CSI) either by feedback from the receiver (mostly UE), in FDD systems [10], or transmitters can reciprocate the channel, in TDD systems [10]. The feedback and reciprocity are valid and practical as long as the feedback has a reasonable overhead and coherence time of the RF channel is larger than the two-way communication time, respectively.

In the case of radars sharing their spectrum with communications systems one way to get CSI is that radar estimates \mathbf{H}_i based on the training symbols sent by communication receivers (or BSs in this case) [11]. Another approach is that radar aids communication systems in channel estimation, with the help of a low-power reference signal, and they feed back the estimated channel to radar [12]. Since, radar signal is treated as interference at communication system, we can characterize the channel as interference channel and refer to information about it as interference-channel state information (ICSI).

Spectrum sharing between radars and communications systems can be envisioned in two domains: military radars sharing spectrum with military communication systems, we call it *Mil2Mil* sharing; another possibility is military radars sharing spectrum with commercial communication systems, we call it *Mil2Com* sharing. In *Mil2Mil* sharing, ICSI can be acquired by radars fairly easily as both systems belong to military. In *Mil2Com* sharing, ICSI can be acquired by giving incentives to com-

mercial communication system. The biggest incentive in this scenario is null-steering and protection from radar interference. Thus, regardless of the sharing scenario, *Mil2Mil* or *Mil2Com*, we have ICSI for the sake of mitigating radar interference at communication systems.

2.2 Radar-Cellular System Spectrum Sharing

After introducing our radar and cellular system models we can now discuss the spectrum sharing scenario between radar and cellular system. In our sharing architecture, MIMO radar and cellular systems are the co-primary users of the 3550–3650 MHz band under consideration. In the following sections, we will discuss the architecture of spectrum sharing problem which is followed by our spectrum sharing algorithm.

2.2.1 Architecture

We illustrate our coexistence scenario in Fig. 2.1 where the maritime MIMO radar is sharing \mathcal{K} interference channels with the cellular system. Considering this scenario, the received signal at the i^{th} BS receiver can be written as

$$\mathbf{r}_i(t) = \mathbf{H}_i^{N^{\text{BS}} \times M} \mathbf{x}(t) + \sum_j \mathbf{H}_j^{N^{\text{BS}} \times N^{\text{UE}}} \mathbf{s}_j^{\text{UE}}(t) + \mathbf{w}(t). \quad (2.10)$$

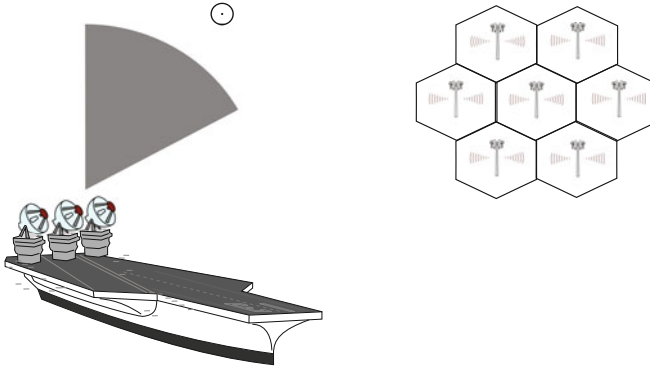


Fig. 2.1 Spectrum sharing scenario: A seaborne MIMO radar detecting a point target while simultaneously sharing spectrum with a MIMO cellular system without causing interference to the cellular system

The goal of the MIMO radar is to map $\mathbf{x}(t)$ onto the null-space of \mathbf{H}_i in order to avoid interference to the i^{th} BS, i.e., $\mathbf{H}_i \mathbf{x}(t) = \mathbf{0}$, so that $\mathbf{r}_i(t)$ has Eq. (2.8) instead of Eq. (2.10).

2.3 Spectrum Sharing Algorithms for Small MIMO Radar

In this section, we discuss performance metrics of spectrum sharing MIMO radars when a MIMO radar has a smaller antenna array as compared to a cellular base station (BS), i.e., $M_T \leq N_R$. We consider the spectrum sharing between a MIMO radar and an LTE cellular system with \mathcal{K} BSs. The MIMO radar and LTE share \mathcal{K} interference channels, i.e., $\mathbf{H}_i, i = 1, 2, \dots, \mathcal{K}$. We propose projecting the radar signal onto the null space of interference channel between the MIMO radar and LTE using our proposed interference-channel-selection algorithm, in order to have zero-interference from the MIMO radar. We select interference channel with the maximum null space, i.e., $\arg\max_{1 \leq i \leq \mathcal{K}} \dim[\mathcal{N}(\mathbf{H}_i)]$ and project the radar signal onto the null space of this channel. Our proposed spatial spectrum sharing algorithm is radar-centric such that it causes minimum loss in radar performance by carefully selecting the interference channel and at the same time protects the i^{th} LTE BS from the radar interference. Through our analytical and simulation results we show that the loss in the radar performance is less when the proposed interference-channel-selection algorithm is used to select the channel onto which radar signals are projected.

2.3.1 Performance Metrics

We choose the Cram r Rao bound (CRB) and maximum likelihood (ML) estimate of the target's angle of arrival as our performance metric for the MIMO radar system. We are interested in studying the degradation in the estimate of the target's angle of arrival due to null-space projection of the radar waveform. The CRB for a single target, no-interference case, is given as in [4],

$$\text{CRB}(\theta) = \frac{1}{2 \text{SNR}} \left(M_R \dot{\mathbf{a}}_T^H(\theta) \mathbf{R}_x^T \dot{\mathbf{a}}_T(\theta) + \mathbf{a}_T^H(\theta) \mathbf{R}_x^T \mathbf{a}_T(\theta) \|\dot{\mathbf{a}}_R(\theta)\|^2 - \frac{M_R |\mathbf{a}_T^H(\theta) \mathbf{R}_x^T \dot{\mathbf{a}}_T(\theta)|^2}{\mathbf{a}_T^H(\theta) \mathbf{R}_x^T \mathbf{a}_T(\theta)} \right)^{-1} \quad (2.11)$$

and the ML for the case of no interference and a single target can be written as in [4],

$$(\hat{\theta}, \hat{\tau}_r, \hat{\omega}_D)_{\text{ML}} = \arg \max_{\theta, \tau_r, \omega_D} \frac{|\mathbf{a}_R^H(\theta) \mathbf{E}(\tau_r, \omega_D) \mathbf{a}_T^*(\theta)|^2}{M_R \mathbf{a}_T^H(\theta) \mathbf{R}_x^T \mathbf{a}_T(\theta)} \quad (2.12)$$

where

$$\begin{aligned}\dot{\mathbf{a}}_R(\theta) &= \frac{d\mathbf{a}_R(\theta)}{d\theta} \\ \dot{\mathbf{a}}_T(\theta) &= \frac{d\mathbf{a}_T(\theta)}{d\theta} \\ \mathbf{R}_x &= \int_{T_0} \mathbf{x}(t) \mathbf{x}^H(t) dt \\ \mathbf{E}(\tau_r, \omega_D) &= \int_{T_0} \mathbf{y}(t) \mathbf{x}^H(t - \tau_r) e^{j\omega_D t} dt\end{aligned}$$

τ_r is the propagation delay, two-way, between the target and the reference point, and ω_D is the Doppler frequency shift.

In addition to performance metrics like CRB and ML, we are also interested in the changes in beampatterns of the MIMO radar due to null-space projection of the radar waveform. Beampattern is a measure of beamformer's response to a target at direction θ given by, as in [4],

$$G(\theta, \theta_D) = \Gamma \frac{|\mathbf{a}_T^H(\theta) \mathbf{R}_x^T \mathbf{a}_T(\theta_D)|^2}{\mathbf{a}_T^H(\theta_D) \mathbf{R}_x^T \mathbf{a}_T(\theta_D)} \frac{|\mathbf{a}_R^H(\theta) \mathbf{a}_R(\theta_D)|^2}{M_R} \quad (2.13)$$

where Γ is the normalization constant and θ_D represents the digital steering direction of the main beam.

2.3.2 Interference-Channel-Selection Algorithm

In this section, we propose our interference-channel-selection algorithm, shown in Algorithm 1, which selects interference channel onto which radar signals are projected using NSP method, i.e., Algorithm 2. We assume there exist \mathcal{K} interference channels, i.e., $\mathbf{H}_i, i = 1, 2, \dots, \mathcal{K}$, between the MIMO radar and the LTE system and we seek to select the best interference channel, defined as

$$\begin{aligned}i_{\max} &\triangleq \underset{1 \leq i \leq \mathcal{K}}{\operatorname{argmax}} \dim[\mathcal{N}(\mathbf{H}_i)] \\ \mathbf{H}_{\text{Best}} &\triangleq \mathbf{H}_{i_{\max}}\end{aligned}$$

and we seek to avoid the worst channel, defined as

$$\begin{aligned}i_{\min} &\triangleq \underset{1 \leq i \leq \mathcal{K}}{\operatorname{argmin}} \dim[\mathcal{N}(\mathbf{H}_i)] \\ \mathbf{H}_{\text{Worst}} &\triangleq \mathbf{H}_{i_{\min}}\end{aligned}$$

where null space of $\mathbf{H}_i^{N_R \times M_T}$ is defined as

$$\mathcal{N}(\mathbf{H}_i) \triangleq \{\mathbf{x} \in \mathbb{C}^{M_T} : \mathbf{H}_i \mathbf{x} = \mathbf{0}\}$$

and then null of $\mathbf{H}_i^{N_R \times M_T}$ is defined as

$$\text{null } \mathbf{H}_i \triangleq \dim[\mathcal{N}(\mathbf{H}_i)]$$

where ‘dim’ is the number of linearly independent columns in null space of $\mathbf{H}_i^{N_R \times M_T}$.

At the MIMO radar, we first estimate the channel state information (CSI) of the \mathcal{K} interference channels using a blind null-space learning algorithm [13]. This is followed by the calculation of null space of these \mathcal{K} interference channels via Algorithm 2. Once Algorithm 1 receives null space of interference channels, it selects channel with the maximum null space as the candidate channel, i.e., $\check{\mathbf{H}}$ and sends it to Algorithm 2 for NSP of radar signals. Our interference-channel-selection algorithm, i.e., Algorithm 1 guarantees minimum degradation in radar performance and at the same time assures zero-interference to the candidate BS.

Algorithm 1 Interference-Channel-Selection Algorithm

```

loop
  for  $i = 1 : \mathcal{K}$  do
    Estimate CSI of  $\mathbf{H}_i$ .
    Send  $\mathbf{H}_i$  to Algorithm 2 for null space computation.
    Receive  $\dim[\mathcal{N}(\mathbf{H}_i)]$  from Algorithm 2.
  end for
  Find  $i_{\max} = \underset{1 \leq i \leq \mathcal{K}}{\text{argmax}} \dim[\mathcal{N}(\mathbf{H}_i)]$ .
  Set  $\check{\mathbf{H}} = \mathbf{H}_{i_{\max}}$  as the candidate interference channel.
  Send  $\check{\mathbf{H}}$  to Algorithm 2 to get NSP radar waveform.
end loop

```

2.3.3 Modified-Null-Space Projection (NSP) Algorithm

In this section, we explain the projection of radar signals onto null space of interference channel selected using Algorithm 1. As mentioned earlier, the CSI of \mathcal{K} interference channels is estimated using a blind null-space learning algorithm [13]. After getting CSI estimates of \mathcal{K} interference channels, from Algorithm 1, the next step is to find null space of each $\mathbf{H}_i^{N_R \times M_T}$ using Algorithm 2. This step is performed using the singular value decomposition (SVD) theorem according to our modified-NSP projection algorithm, as shown in Algorithm 2. For the complex i^{th} interference channel matrix the SVD is given as

$$\begin{aligned}
\mathbf{H}_i^{N_R \times M_T} &= \mathbf{U}_i \boldsymbol{\Sigma}_i^{N_R \times M_T} \mathbf{V}_i^H \\
&= \mathbf{U}_i \begin{pmatrix} \sigma_1 & & & \\ & \sigma_2 & & 0 \\ & & \ddots & \\ 0 & & & \sigma_{j \in \min(N_R, M_T)} \end{pmatrix} \mathbf{V}_i^H
\end{aligned}$$

where \mathbf{U}_i is the complex unitary matrix, $\boldsymbol{\Sigma}_i$ is the diagonal matrix of singular values, and \mathbf{V}_i^H is the complex unitary matrix. If the SVD analysis do not yield any zero singular values we resort to a numerical approach to calculate null space. In order to do that, in Algorithm 2, we set a threshold δ and select singular values below the threshold value. Then the number of singular values below the threshold serves as the dimension of null space.

Algorithm 2 Modified-Null-Space Projection (NSP)

```

if  $\mathbf{H}_i$  received from Algorithm 1 then
  Perform SVD on  $\mathbf{H}_i$  (i.e.,  $\mathbf{H}_i = \mathbf{U}_i \boldsymbol{\Sigma}_i \mathbf{V}_i^H$ )
  if  $\sigma_j \neq 0$  (i.e.,  $j^{\text{th}}$  singular value of  $\boldsymbol{\Sigma}_i$ ) then
     $\dim[\mathcal{N}(\mathbf{H}_i)] = 0$ 
    Use pre-specified threshold  $\delta$ 
    for  $j = 1 : \min(N_R, M_T)$  do
      if  $\sigma_j < \delta$  then
         $\dim[\mathcal{N}(\mathbf{H}_i)] = \dim[\mathcal{N}(\mathbf{H}_i)] + 1$ 
      else
         $\dim[\mathcal{N}(\mathbf{H}_i)] = 0$ 
      end if
    end for
  else
     $\dim[\mathcal{N}(\mathbf{H}_i)] = \text{The number of zero singular values}$ 
  end if
  Send  $\dim[\mathcal{N}(\mathbf{H}_i)]$  to Algorithm 1.
end if
if  $\check{\mathbf{H}}$  received from Algorithm 1 then
  Perform SVD on  $\check{\mathbf{H}} = \mathbf{U} \boldsymbol{\Sigma} \mathbf{V}$ 
  if  $\sigma_j \neq 0$  then
    Use pre-specified threshold  $\delta$ 
     $\sigma_{\text{Null}} = \{ \}$  {An empty set to collect  $\sigma$ s below threshold  $\delta$ }
    for  $j = 1 : \min(N_R, M_T)$  do
      if  $\sigma_j < \delta$  then
        Add  $\sigma_j$  to  $\sigma_{\text{Null}}$ 
      end if
    end for
     $\check{\mathbf{V}} = \sigma_{\text{Null}}$  corresponding columns in  $\mathbf{V}$ .
  end if
  Setup projection matrix  $\mathbf{P}_{\check{\mathbf{V}}} = \check{\mathbf{V}}\check{\mathbf{V}}^H$ .
  Get NSP radar signal via  $\check{\mathbf{x}} = \mathbf{P}_{\check{\mathbf{V}}}\mathbf{x}$ .
end if

```

Once the null space of all interference channels is determined we seek to find the best channel $\check{\mathbf{H}}$, the one with the maximum null space, which according to our Algorithm 1 is given as

$$i_{\max} = \underset{1 \leq i \leq \mathcal{K}}{\operatorname{argmax}} \dim \mathcal{N}(\mathbf{H}_i)$$

$$\check{\mathbf{H}} = \mathbf{H}_{i_{\max}}$$

Algorithm 1 sends $\check{\mathbf{H}}$ to Algorithm 2 for null-space computation, where after SVD the right singular vectors corresponding to vanishing singular are collected in $\check{\mathbf{V}}$ for the formation of projection matrix. Once this is done, we project the radar signal onto the null space of \mathbf{H}_{Best} via a modified version of our projection algorithm [5, 14]. The proposed NSP algorithm removes redundancy from previous algorithm and is computationally efficient. The modified-NSP algorithm is given as

$$\mathbf{P}_{\check{\mathbf{V}}} = \check{\mathbf{V}}\check{\mathbf{V}}^H.$$

The radar waveform projected onto null space of $\check{\mathbf{H}}$ can be written as

$$\check{\mathbf{x}} = \mathbf{P}_{\check{\mathbf{V}}} \mathbf{x}. \quad (2.14)$$

By inserting the projected signal, as in Eq. (2.14), into the Cramer–Rao bound (CRB) for the single target no interference case, Eq. (2.11), we get the CRB for the NSP projected radar waveform as

$$\text{CRB}_{\text{NSP}}(\theta) = \frac{1}{2 \text{SNR}} \left(M_R \dot{\mathbf{a}}_T^H(\theta) \mathbf{R}_{\check{\mathbf{x}}}^T \dot{\mathbf{a}}_T(\theta) + \mathbf{a}_T^H(\theta) \right. \\ \left. \mathbf{R}_{\check{\mathbf{x}}}^T \mathbf{a}_T(\theta) \|\dot{\mathbf{a}}_R(\theta)\|^2 - \frac{M_R |\mathbf{a}_T^H(\theta) \mathbf{R}_{\check{\mathbf{x}}}^T \dot{\mathbf{a}}_T(\theta)|^2}{\mathbf{a}_T^H(\theta) \mathbf{R}_{\check{\mathbf{x}}}^T \mathbf{a}_T(\theta)} \right)^{-1}. \quad (2.15)$$

Similarly, Eq. (2.14) can be substituted in (2.12) to get the ML estimate of angle arrival for the NSP projected radar waveform as

$$(\hat{\theta}, \hat{\tau}_r, \hat{\omega}_D)_{\text{MLNSP}} = \arg \max_{\theta, \tau_r, \omega_D} \frac{|\mathbf{a}_R^H(\theta) \mathbf{E}(\tau_r, \omega_D) \mathbf{a}_T^*(\theta)|^2}{M_R \mathbf{a}_T^H(\theta) \mathbf{R}_{\check{\mathbf{x}}}^T \mathbf{a}_T(\theta)}. \quad (2.16)$$

In order to analyze the beampattern of the NSP projected waveform we can substitute Eq. (2.14) in Eq. (2.13) to get

$$G_{\text{NSP}}(\theta, \theta_D) = \Gamma \frac{|\mathbf{a}_T^H(\theta) \mathbf{R}_{\check{\mathbf{x}}}^T \mathbf{a}_T(\theta_D)|^2 |\mathbf{a}_R^H(\theta) \mathbf{a}_R(\theta_D)|^2}{\mathbf{a}_T^H(\theta_D) \mathbf{R}_{\check{\mathbf{x}}}^T \mathbf{a}_T(\theta_D) M_R}. \quad (2.17)$$

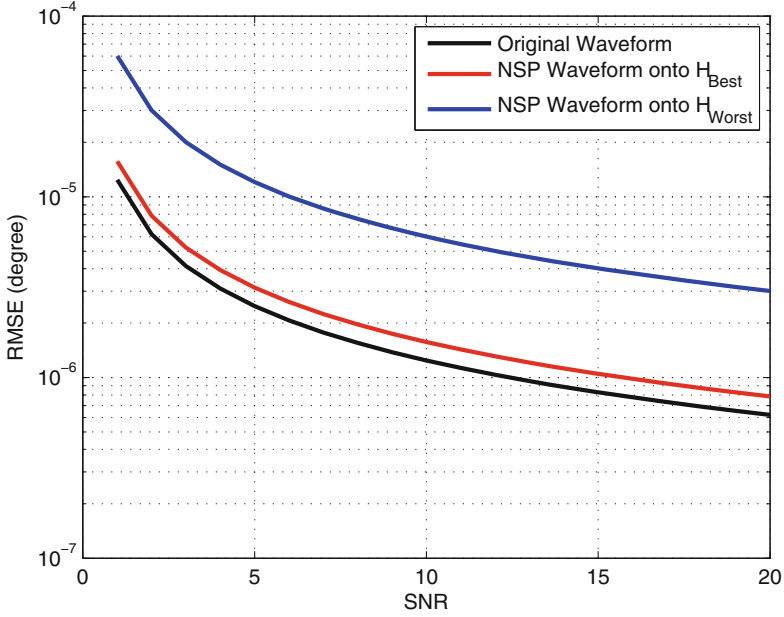


Fig. 2.2 CRB on target direction estimation RMSE as a function of the SNR. H_{Best} and H_{Worst} channels are selected using Algorithms 1 and 2

2.3.4 Simulation Results

In this section, we simulate our MIMO radar-LTE sharing scenario and study its impact on the performance of radar.

The CRB for the target's angle of arrival is given by Eqs. (2.11) and (2.15) for the original radar waveform and the NSP radar waveform, respectively. We are interested in understanding the effects of NSP on the radar waveform. In Fig. 2.2, we compare the root-mean-square-error (RMSE) of different radar waveforms. We compare the performance of original radar waveform with the NSP waveform projected onto H_{Best} and H_{Worst} . Note that by using Algorithms 1 and 2 we are able to minimize degradation in the radar performance as the NSP waveform onto H_{Best} is closer to the original radar waveform in RMSE sense than the NSP waveform onto H_{Worst} . Thus, by an appropriate selection of the interference-channel degradation in the radar performance, due to the NSP of its waveform, can be minimized.

Similar to the CRB, the ML estimate of the target's angle of arrival is given by Eqs. (2.12) and (2.16) for the original radar waveform and the NSP radar waveform, respectively. We are interested in the estimation error of the angle due to the NSP of radar waveform. In Fig. 2.3, we compare original angles and estimated angles using ML estimation for different radar waveforms. Using Algorithms 1 and 2 we can achieve almost similar ML results for original waveform and the NSP waveform

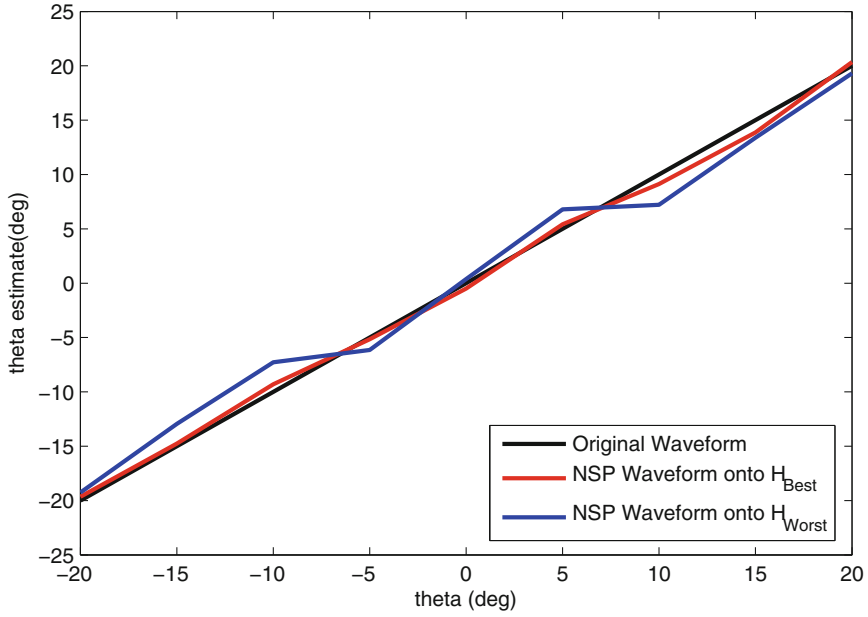


Fig. 2.3 ML on target direction estimation. H_{Best} and H_{Worst} channels are selected using Algorithms 1 and 2

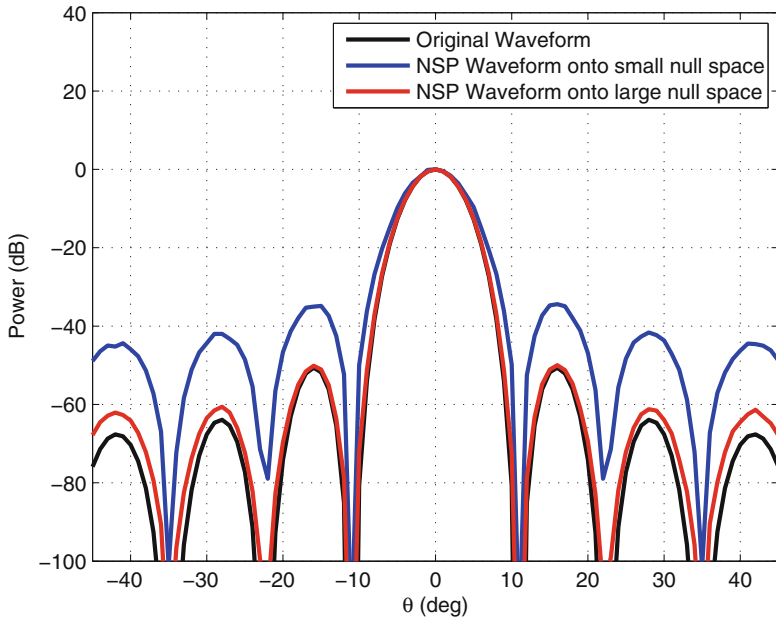


Fig. 2.4 Beam pattern of MIMO radar when different values of threshold are used to calculate the null space of interference channels in Algorithm 2

which shows that by choosing \mathbf{H}_{Best} to project we can cause minimum degradation in radar performance. Note that the ML estimate for the NSP waveform onto $\mathbf{H}_{\text{Worst}}$ is much degraded from the original waveform and the NSP waveform onto \mathbf{H}_{Best} .

In Algorithm 2, we describe an approach to numerically calculate null space of interference channels. This is an important approach in the presence of rounding errors and fuzzy data. We select singular values below a certain threshold and take the corresponding columns of \mathbf{V}_i^H for our NSP equation. Thus, the value of threshold can be a limitation parameter in the projection algorithm, since, the bigger the value of threshold the bigger the null space and the better the performance of the NSP radar waveform. This can be easily noticed from Fig. 2.4, where we compare the beam pattern of original radar waveform with the NSP waveform when we choose a larger and a smaller value of threshold. The larger value of threshold corresponds to the best channel and the smaller value corresponds to the worst channel, according to our definitions in Sect. 2.3.2. Note that by increasing or decreasing the value of threshold we can manipulate the magnitude of sidelobes. Thus, for the best radar performance, it is desirable to select interference channel with the maximum null space, i.e., according to Algorithms 1 and 2.

2.4 Spectrum Sharing Algorithms for Large MIMO Radar

In this section, we address the problem of target detection by radars that project waveform onto the null space of interference channel in order to mitigate interference to cellular systems. We consider a multiple-input multiple-output (MIMO) radar and a MIMO cellular communication system with \mathcal{K} base stations (BS). We consider two spectrum sharing scenarios. In the first scenario, the degrees of freedom (DoF) available at the radar are not sufficient enough to simultaneously detect target and mitigate interference to \mathcal{K} BSs. For this case, we select one BS among \mathcal{K} BSs for waveform projection on the basis of guaranteeing minimum waveform degradation. For the second case, the radar has sufficient DoF to simultaneously detect target and mitigate interference to all \mathcal{K} BSs. We study target detection capabilities of null-space projected (NSP) waveform and compare it with the orthogonal waveform. We derive the generalized likelihood ratio test (GLRT) for target detection and derive detector statistic for NSP and orthogonal waveform. The target detection performance for both waveforms is studied theoretically and via Monte Carlo simulations.

We consider two spectrum sharing scenarios which are discussed as follows.

Case 1 ($M \ll \mathcal{K}N^{\text{BS}}$ but $M > N^{\text{BS}}$): Consider a scenario in which a MIMO radar has a very small antenna array as compared to the combined antenna array of \mathcal{K} BSs, i.e., $M \ll \mathcal{K}N^{\text{BS}}$, but is larger than individual BS antenna array, i.e., $M > N^{\text{BS}}$. In such a scenario, it is not possible for the MIMO radar to simultaneously mitigate interference to all the \mathcal{K} BSs present in the network because of insufficient degrees of freedom (DoF) available. However, the available DoF allow simultaneous target detection and interference mitigation to one of the BS among \mathcal{K} BSs. The choice of BS selection depends upon the performance metric which radar wants to optimize.

In this chapter, our performance metric is minimum degradation of radar waveform in a minimum norm sense.

A drawback of this approach is that interference is not mitigated to $\mathcal{K} - 1$ BSs present in the network and the radar has to utilize higher transmit power to achieve the same performance level which can increase the level of interference at BSs not part of the mitigation scheme. This drawback is addressed in the literature by moving $\mathcal{K} - 1$ BSs to non-radar frequency bands by using resource allocation and carrier aggregation techniques [15, 16].

It is worth mentioning that when $M \ll \mathcal{K}N^{\text{BS}}$ traditional colocated MIMO radar architecture is not suitable for mitigation of interference by using NSP approaches because sufficient DoF are not available and doing so will result in performance degradation of radar systems. However, the MIMO radar architecture can be modified into an overlapped-MIMO radar architecture, where the transmit array of colocated MIMO radar is partitioned into a number of subarrays that are allowed to overlap. The overlapped-MIMO radar architecture increases the DoF and enjoys the advantages of the MIMO radar while mitigating interference to communication systems without sacrificing the main desirable characteristics for its own transmission.

Case 2 ($M \gg \mathcal{K}N^{\text{BS}}$): Consider a scenario in which a MIMO radar has a very large antenna array as compared to the combined antenna array of \mathcal{K} BSs, i.e., $M \gg \mathcal{K}N^{\text{BS}}$. In such a scenario, it is feasible for the MIMO radar to simultaneously mitigate interference to all the \mathcal{K} BSs present in the network while reliably detecting targets. This is because sufficient degrees of freedom are available for both the tasks. In such a scenario, the combined interference channel that the MIMO radar shares with \mathcal{K} BSs in the networks is given as

$$\mathbf{H} = [\mathbf{H}_1 \ \mathbf{H}_2 \ \cdots \ \mathbf{H}_{\mathcal{K}}]. \quad (2.18)$$

2.4.1 Projection Matrix

In this section, we introduce formation of projection matrices for Case 1 and Case 2.

Projection for Case 1 ($M \ll \mathcal{K}N^{\text{BS}}$ but $M > N^{\text{BS}}$): In this section, we define the projection algorithm for ‘Case 1’ which projects radar signal onto the null space of interference channel \mathbf{H}_i . Assuming, the MIMO radar has channel state information of all \mathbf{H}_i interference channels, through feedback, in *Mil2Mil* or *Mil2Com* scenario, we can perform singular value decomposition (SVD) to find the null space and then construct a projector matrix. We proceed by first finding SVD of \mathbf{H}_i , i.e.,

$$\mathbf{H}_i = \mathbf{U}_i \boldsymbol{\Sigma}_i \mathbf{V}_i^H. \quad (2.19)$$

Now, let us define

$$\tilde{\boldsymbol{\Sigma}}_i \triangleq \text{diag}(\tilde{\sigma}_{i,1}, \tilde{\sigma}_{i,2}, \dots, \tilde{\sigma}_{i,p}) \quad (2.20)$$

where $p \triangleq \min(N^{\text{BS}}, M)$ and $\tilde{\sigma}_{i,1} > \tilde{\sigma}_{i,2} > \dots > \tilde{\sigma}_{i,q} > \tilde{\sigma}_{i,q+1} = \tilde{\sigma}_{i,q+2} = \dots = \tilde{\sigma}_{i,p} = 0$ are the singular values of \mathbf{H}_i . Next, we define

$$\tilde{\Sigma}'_i \triangleq \text{diag}(\tilde{\sigma}'_{i,1}, \tilde{\sigma}'_{i,2}, \dots, \tilde{\sigma}'_{i,M}) \quad (2.21)$$

where

$$\tilde{\sigma}'_{i,u} \triangleq \begin{cases} 0, & \text{for } u \leq q, \\ 1, & \text{for } u > q. \end{cases} \quad (2.22)$$

Using above definitions we can now define our projection matrix, i.e.,

$$\mathbf{P}_i \triangleq \mathbf{V}_i \tilde{\Sigma}'_i \mathbf{V}_i^H. \quad (2.23)$$

In order to show that \mathbf{P}_i is a valid projection matrix we prove two results on projection matrices below.

Property 2.1 $\mathbf{P}_i \in \mathbb{C}^{M \times M}$ is a projection matrix if and only if $\mathbf{P}_i = \mathbf{P}_i^H = \mathbf{P}_i^2$.

Proof Let's start by showing the 'only if' part. First, we show $\mathbf{P}_i = \mathbf{P}_i^H$. Taking Hermitian of Eq. (2.23) we have

$$\mathbf{P}_i^H = (\mathbf{V}_i \tilde{\Sigma}'_i \mathbf{V}_i^H)^H = \mathbf{P}_i. \quad (2.24)$$

Now, squaring Eq. (2.23) we have

$$\mathbf{P}_i^2 = \mathbf{V}_i \tilde{\Sigma}'_i \mathbf{V}_i^H \times \mathbf{V}_i \tilde{\Sigma}'_i \mathbf{V}_i^H = \mathbf{P}_i \quad (2.25)$$

where above equation follows from $\mathbf{V}_i^H \mathbf{V}_i = \mathbf{I}$ (since they are orthonormal matrices) and $(\tilde{\Sigma}'_i)^2 = \tilde{\Sigma}'_i$ (by construction). From Eqs. (2.24) and (2.25) it follows that $\mathbf{P}_i = \mathbf{P}_i^H = \mathbf{P}_i^2$. Next, we show \mathbf{P}_i is a projector by showing that if $\mathbf{v} \in \text{range}(\mathbf{P}_i)$, then $\mathbf{P}_i \mathbf{v} = \mathbf{v}$, i.e., for some \mathbf{w} , $\mathbf{v} = \mathbf{P}_i \mathbf{w}$, then

$$\mathbf{P}_i \mathbf{v} = \mathbf{P}_i (\mathbf{P}_i \mathbf{w}) = \mathbf{P}_i^2 \mathbf{w} = \mathbf{P}_i \mathbf{w} = \mathbf{v}. \quad (2.26)$$

Moreover, $\mathbf{P}_i \mathbf{v} - \mathbf{v} \in \text{null}(\mathbf{P}_i)$, i.e.,

$$\mathbf{P}_i (\mathbf{P}_i \mathbf{v} - \mathbf{v}) = \mathbf{P}_i^2 \mathbf{v} - \mathbf{P}_i \mathbf{v} = \mathbf{P}_i \mathbf{v} - \mathbf{P}_i \mathbf{v} = \mathbf{0}. \quad (2.27)$$

This concludes our proof.

Property 2.2 $\mathbf{P}_i \in \mathbb{C}^{M \times M}$ is an orthogonal projection matrix onto the null space of $\mathbf{H}_i \in \mathbb{C}^{N^{\text{BS}} \times M}$.

Proof Since $\mathbf{P}_i = \mathbf{P}_i^H$, we can write

$$\mathbf{H}_i \mathbf{P}_i^H = \mathbf{U}_i \tilde{\mathbf{\Sigma}}_i \mathbf{V}_i^H \times \mathbf{V}_i \tilde{\mathbf{\Sigma}}_i' \mathbf{V}_i^H = \mathbf{0}. \quad (2.28)$$

The above results follows from noting that $\tilde{\mathbf{\Sigma}}_i \tilde{\mathbf{\Sigma}}_i' = \mathbf{0}$ by construction.

For ‘Case 1’ we are dealing with \mathcal{K} interference channels. Therefore, we need to select the interference channel which results in least degradation of radar waveform in a minimum norm sense, i.e.,

$$i_{\min} \triangleq \underset{1 \leq i \leq \mathcal{K}}{\operatorname{argmin}} \left\| \mathbf{P}_i \mathbf{x}(t) - \mathbf{x}(t) \right\|_2 \quad (2.29)$$

$$\check{\mathbf{P}} \triangleq \mathbf{P}_{i_{\min}}. \quad (2.30)$$

Once we have selected our projection matrix it is straight forward to project radar signal onto the null space of interference channel via

$$\check{\mathbf{x}}(t) = \check{\mathbf{P}} \mathbf{x}(t). \quad (2.31)$$

The correlation matrix of our NSP waveform is given as

$$\mathbf{R}_{\check{\mathbf{x}}} = \int_{T_o} \check{\mathbf{x}}(t) \check{\mathbf{x}}^H(t) dt \quad (2.32)$$

which is no longer identity, because the projection does not preserve the orthogonality, and its rank depends upon the rank of the projection matrix.

Projection for Case 2 ($M \gg \mathcal{K} N^{\text{BS}}$): In this section, we define the projection algorithm for ‘Case 2’ which projects radar signal onto the null space of combined interference channel \mathbf{H} . The SVD of \mathbf{H} is given as

$$\mathbf{H} = \mathbf{U} \mathbf{\Sigma} \mathbf{V}^H. \quad (2.33)$$

Now, let us define

$$\tilde{\mathbf{\Sigma}} \triangleq \operatorname{diag}(\tilde{\sigma}_1, \tilde{\sigma}_2, \dots, \tilde{\sigma}_p) \quad (2.34)$$

where $p \triangleq \min(N^{\text{BS}}, M)$ and $\tilde{\sigma}_1 > \tilde{\sigma}_2 > \dots > \tilde{\sigma}_q > \tilde{\sigma}_{q+1} = \tilde{\sigma}_{q+2} = \dots = \tilde{\sigma}_p = 0$ are the singular values of \mathbf{H} . Next, we define

$$\tilde{\mathbf{\Sigma}}_i' \triangleq \operatorname{diag}(\tilde{\sigma}'_1, \tilde{\sigma}'_2, \dots, \tilde{\sigma}'_M) \quad (2.35)$$

where

$$\tilde{\sigma}'_u \triangleq \begin{cases} 0, & \text{for } u \leq q, \\ 1, & \text{for } u > q. \end{cases} \quad (2.36)$$

Using above definitions we can now define our projection matrix, i.e.,

$$\mathbf{P} \triangleq \mathbf{V} \tilde{\Sigma}' \mathbf{V}^H. \quad (2.37)$$

It is straightforward to see that \mathbf{P} is a valid projection matrix by using Properties 1 and 2.

2.4.2 Spectrum Sharing and Projection Algorithms

In this section, we explain spectrum sharing and projection algorithms for ‘Case 1’ and ‘Case 2’.

Algorithms for Case 1 ($M \ll \mathcal{K}N^{\text{BS}}$ but $M > N^{\text{BS}}$): For this case, the process of spectrum sharing by forming projection matrices and selecting interference channels is executed with the help of Algorithms 3 and 4. First, at each pulse repetition interval (PRI), the radar obtains ICSI of all \mathcal{K} interference channels. This information is sent to Algorithm 4 for the calculation of null spaces and formation of projection matrices. Algorithm 3 process \mathcal{K} projection matrices, received from Algorithm 4, to find the projection matrix which results in least degradation of radar waveform in a minimum norm sense. This step is followed by the projection of radar waveform onto the null space of the selected BS, i.e., the BS to the corresponding selected projection matrix, and waveform transmission.

Algorithm 3 Spectrum Sharing Algorithm for Case 1

```

loop
  for  $i = 1 : \mathcal{K}$  do
    Get CSI of  $\mathbf{H}_i$  through feedback from the  $i^{\text{th}}$  BS.
    Send  $\mathbf{H}_i$  to Algorithm 4 for the formation of projection matrix  $\mathbf{P}_i$ .
    Receive the  $i^{\text{th}}$  projection matrix  $\mathbf{P}_i$  from Algorithm 4.
  end for
  Find  $i_{\min} = \underset{1 \leq i \leq \mathcal{K}}{\operatorname{argmin}} \left\| \mathbf{P}_i \mathbf{x}(t) - \mathbf{x}(t) \right\|_2$ .
  Set  $\check{\mathbf{P}} = \mathbf{P}_{i_{\min}}$  as the desired projector.
  Perform null space projection, i.e.,  $\check{\mathbf{x}}(t) = \check{\mathbf{P}} \mathbf{x}(t)$ .
end loop

```

Projection for Case 2 ($M \gg \mathcal{K}N^{\text{BS}}$): For this case, the process of spectrum sharing is executed with the help of Algorithms 5 and 6. First, at each pulse repetition interval (PRI), the radar obtains ICSI of all \mathcal{K} interference channels. This information is sent to Algorithm 6 for the calculation of null space of \mathbf{H} and the formation of projection matrix \mathbf{P} . The projection of radar waveform onto the null space of \mathbf{H} is performed by Algorithm 5.

Algorithm 4 Projection Algorithm for Case 1

```

if  $\mathbf{H}_i$  received from Algorithm 3 then
  Perform SVD on  $\mathbf{H}_i$  (i.e.,  $\mathbf{H}_i = \mathbf{U}_i \boldsymbol{\Sigma}_i \mathbf{V}_i^H$ )
  Construct  $\tilde{\boldsymbol{\Sigma}}_i = \text{diag}(\tilde{\sigma}_{i,1}, \tilde{\sigma}_{i,2}, \dots, \tilde{\sigma}_{i,p})$ 
  Construct  $\tilde{\boldsymbol{\Sigma}}'_i = \text{diag}(\tilde{\sigma}'_{i,1}, \tilde{\sigma}'_{i,2}, \dots, \tilde{\sigma}'_{i,M})$ 
  Setup projection matrix  $\mathbf{P}_i = \mathbf{V}_i \tilde{\boldsymbol{\Sigma}}'_i \mathbf{V}_i^H$ .
  Send  $\mathbf{P}_i$  to Algorithm 3.
end if

```

Algorithm 5 Spectrum Sharing Algorithm for Case 2

```

loop
  Get CSI of  $\mathbf{H}$  through feedback from  $\mathcal{K}$  BSs.
  Send  $\mathbf{H}$  to Algorithm 6 for the formation of projection matrix  $\mathbf{P}$ .
  Receive the projection matrix  $\mathbf{P}$  from Algorithm 6.
  Perform null space projection, i.e.,  $\tilde{\mathbf{x}}(t) = \mathbf{P}\mathbf{x}(t)$ .
end loop

```

Algorithm 6 Projection Algorithm for Case 2

```

if  $\mathbf{H}$  received from Algorithm 5 then
  Perform SVD on  $\mathbf{H}$  (i.e.,  $\mathbf{H} = \mathbf{U} \boldsymbol{\Sigma} \mathbf{V}^H$ )
  Construct  $\tilde{\boldsymbol{\Sigma}} = \text{diag}(\tilde{\sigma}_1, \tilde{\sigma}_2, \dots, \tilde{\sigma}_p)$ 
  Construct  $\tilde{\boldsymbol{\Sigma}}'_i = \text{diag}(\tilde{\sigma}'_1, \tilde{\sigma}'_2, \dots, \tilde{\sigma}'_M)$ 
  Setup projection matrix  $\mathbf{P} = \mathbf{V} \tilde{\boldsymbol{\Sigma}}'_i \mathbf{V}^H$ .
  Send  $\mathbf{P}$  to Algorithm 5.
end if

```

2.4.3 Statistical Decision Test for Target Detection

In this section, we develop a statistical decision test for target illuminated with the orthogonal radar waveforms and the NSP projected radar waveforms. The goal is to compare performance of the two waveforms by looking at the test decision on whether the target is present or not in the range-Doppler cell of interest.

For target detection and estimation, we proceed by constructing a hypothesis test where we seek to choose between two hypothesis: the null hypothesis \mathcal{H}_0 which represents the case when the target is absent or the alternate hypothesis \mathcal{H}_1 which represents the case when the target is present. The hypothesis for a single target model in Eq. (2.5) can be written as

$$\mathbf{y}(t) = \begin{cases} \mathcal{H}_1 : \alpha \mathbf{A}(\theta) \mathbf{x}(t) + \mathbf{n}(t), & 0 \leq t \leq T_o, \\ \mathcal{H}_0 : \mathbf{n}(t), & 0 \leq t \leq T_o. \end{cases} \quad (2.38)$$

Since, θ and α are unknown, but deterministic, we use the generalize likelihood ratio test (GLRT). The advantage of using GLRT is that we can replace the unknown parameters with their maximum likelihood (ML) estimates. The ML estimates of α

and θ are found for various signal models, targets, and interference sources in [4, 17] when using orthogonal signals. In this chapter, we consider a simpler model with one target and no interference sources in order to study the impact of NSP on target detection in a tractable manner. Therefore, we present a simpler derivation of the ML estimation and GLRT.

The received signal model in Eq. (2.5) can be written as

$$\mathbf{y}(t) = \mathbf{Q}(t, \theta)\alpha + \mathbf{n}(t) \quad (2.39)$$

where

$$\mathbf{Q}(t, \theta) = \mathbf{A}(\theta)\mathbf{x}(t). \quad (2.40)$$

We use Karhunen–Loève expansion for derivation of the log-likelihood function for estimating θ and α . Let Ω denote the space of the elements of $\{\mathbf{y}(t)\}$, $\{\mathbf{Q}(t, \theta)\}$, and $\{\mathbf{n}(t)\}$. Moreover, let ψ_z , $z = 1, 2, \dots$, be an orthonormal basis function of Ω satisfying

$$\langle \psi_z(t), \psi_{z'}(t) \rangle = \int_{T_0} \psi_z(t) \psi_{z'}^*(t) dt = \delta_{zz'} \quad (2.41)$$

where $\delta_{zz'}$ is the Krönecker delta function. Then, the following series can be used to expand the processes, $\{\mathbf{y}(t)\}$, $\{\mathbf{Q}(t, \theta)\}$, and $\{\mathbf{n}(t)\}$, as

$$\mathbf{y}(t) = \sum_{z=1}^{\infty} \mathbf{y}_z \psi_z(t) \quad (2.42)$$

$$\mathbf{Q}(t, \theta) = \sum_{z=1}^{\infty} \mathbf{Q}_z(\theta) \psi_z(t) \quad (2.43)$$

$$\mathbf{n}(t) = \sum_{z=1}^{\infty} \mathbf{n}_z \psi_z(t) \quad (2.44)$$

where \mathbf{y}_z , \mathbf{Q}_z , and \mathbf{n}_z are coefficients in the Karhunen–Loève expansion of the considered processes obtained by taking the corresponding inner product with basis function $\psi_z(t)$. Thus, an equivalent discrete model of Eq. (2.39) can be obtained as

$$\mathbf{y}_z = \mathbf{Q}_z(\theta)\alpha + \mathbf{n}_z, \quad z = 1, 2, \dots \quad (2.45)$$

For white circular complex Gaussian processes, i.e., $\mathbb{E}[\mathbf{n}(t)\mathbf{n}^*(t - \tau(t))] = \sigma_n^2 \mathbf{I}_M \delta(\tau(t))$, the sequence $\{\mathbf{n}_z\}$ is i.i.d. and $\mathbf{n}_z \sim \mathcal{N}^c(\mathbf{0}_M, \sigma_n^2 \mathbf{I}_M)$. Thus, we can express the log-likelihood function as

$$L_{\mathbf{y}}(\theta, \alpha) = \sum_{z=1}^{\infty} \left(-M \log(\pi \sigma_n^2) - \frac{1}{\sigma_n^2} \|\mathbf{y}_z - \mathbf{Q}_z(\theta)\alpha\|^2 \right). \quad (2.46)$$

Maximizing Eq. (2.46) with respect to α yields

$$L_{\mathbf{y}}(\theta, \hat{\alpha}) = \Gamma - \frac{1}{\sigma_n^2} \left(E_{\mathbf{y}\mathbf{y}} - \mathbf{e}_{\mathbf{Q}\mathbf{y}}^H \mathbf{E}_{\mathbf{Q}\mathbf{Q}}^{-1} \mathbf{e}_{\mathbf{Q}\mathbf{y}} \right) \quad (2.47)$$

where

$$\Gamma \triangleq -M \log(\pi \sigma_n^2) \quad (2.48)$$

$$E_{\mathbf{y}\mathbf{y}} \triangleq \sum_{z=1}^{\infty} \|\mathbf{y}_z\|^2 \quad (2.49)$$

$$\mathbf{e}_{\mathbf{Q}\mathbf{y}} \triangleq \sum_{z=1}^{\infty} \mathbf{Q}_z^H \mathbf{y}_z \quad (2.50)$$

$$\mathbf{E}_{\mathbf{Q}\mathbf{Q}}^{-1} \triangleq \sum_{z=1}^{\infty} \mathbf{Q}_z^H \mathbf{Q}_z. \quad (2.51)$$

Note that, in Eq. (2.47), apart from the constant Γ , the remaining summation goes to infinity. However, due to the noncontribution of higher order terms in the estimation of θ and α the summation can be finite. Using the identity

$$\int_{T_o} \mathbf{v}_1(t) \mathbf{v}_2^H(t) dt = \sum_{z=1}^{\infty} \mathbf{v}_{1z} \mathbf{v}_{2z}^H \quad (2.52)$$

for $\mathbf{v}_i(t) = \sum_{z=1}^{\infty} \mathbf{v}_{1z} \psi_z(t)$, $i = 1, 2$, Eqs. (2.49)–(2.51) can be written as

$$E_{\mathbf{y}\mathbf{y}} \triangleq \int_{T_o} \|\mathbf{y}(t)\|^2 dt \quad (2.53)$$

$$\mathbf{e}_{\mathbf{Q}\mathbf{y}} \triangleq \int_{T_o} \mathbf{Q}^H(t, \theta) \mathbf{y}(t) dt \quad (2.54)$$

$$\mathbf{E}_{\mathbf{Q}\mathbf{Q}} \triangleq \int_{T_o} \mathbf{Q}^H(t, \theta) \mathbf{Q}(t, \theta) dt. \quad (2.55)$$

Using the definition of $\mathbf{Q}(t, \theta)$ in Eq. (2.40), we can write the f^{th} element of $\mathbf{e}_{\mathbf{Q}\mathbf{y}}$ as

$$[\mathbf{e}_{\mathbf{Q}\mathbf{y}}]_f = \mathbf{a}^H(\theta_f) \mathbf{E}^T \mathbf{a}(\theta_f) \quad (2.56)$$

where

$$\mathbf{E} = \int_{T_o} \mathbf{y}(t) \mathbf{x}^H(t) dt. \quad (2.57)$$

Similarly, we can write the fg^{th} element of $\mathbf{E}_{\mathbf{Q}\mathbf{Q}}$ as

$$[\mathbf{E}_{\mathbf{Q}\mathbf{Q}}]_{fg} = \mathbf{a}^H(\theta_f)\mathbf{a}(\theta_g)\mathbf{a}^H(\theta_f)\mathbf{R}_x^T\mathbf{a}(\theta_g). \quad (2.58)$$

Since, $\mathbf{e}_{\mathbf{Q}\mathbf{y}}$ and $\mathbf{E}_{\mathbf{Q}\mathbf{Q}}$ are independent of the received signal, the sufficient statistic to calculate θ and α is given by \mathbf{E} . Using Eqs. (2.56)–(2.58) we can write the ML estimate in matrix-vector form as

$$L_{\mathbf{y}}(\hat{\theta}_{\text{ML}}) = \underset{\theta}{\operatorname{argmax}} \frac{\left| \mathbf{a}^H(\hat{\theta}_{\text{ML}})\mathbf{E}\mathbf{a}^*(\hat{\theta}_{\text{ML}}) \right|^2}{M\mathbf{a}^H(\hat{\theta}_{\text{ML}})\mathbf{R}_x^T\mathbf{a}(\hat{\theta}_{\text{ML}})}. \quad (2.59)$$

Then, the GLRT for our hypothesis testing model in Eq. (2.38) is given as

$$L_{\mathbf{y}} = \max_{\theta, \alpha} \{ \log f_{\mathbf{y}}(\mathbf{y}, \theta, \alpha; \mathcal{H}_1) \} - \log f(\mathbf{y}; \mathcal{H}_0) \underset{\mathcal{H}_0}{\overset{\mathcal{H}_1}{\gtrless}} \delta \quad (2.60)$$

where $f_{\mathbf{y}}(\mathbf{y}, \theta, \alpha; \mathcal{H}_1)$ and $f(\mathbf{y}; \mathcal{H}_0)$ are the probability density functions of the received signal under hypothesis \mathcal{H}_1 and \mathcal{H}_0 , respectively. Hence, the GLRT can be expressed as

$$L_{\mathbf{y}}(\hat{\theta}_{\text{ML}}) = \underset{\theta}{\operatorname{argmax}} \frac{\left| \mathbf{a}^H(\hat{\theta}_{\text{ML}})\mathbf{E}\mathbf{a}^*(\hat{\theta}_{\text{ML}}) \right|^2}{M\mathbf{a}^H(\hat{\theta}_{\text{ML}})\mathbf{R}_x^T\mathbf{a}(\hat{\theta}_{\text{ML}})} \underset{\mathcal{H}_0}{\overset{\mathcal{H}_1}{\gtrless}} \delta. \quad (2.61)$$

The asymptotic statistic of $L(\hat{\theta}_{\text{ML}})$ for both the hypothesis is given by [18]

$$L(\hat{\theta}_{\text{ML}}) \sim \begin{cases} \mathcal{H}_1 : \chi_2^2(\rho), \\ \mathcal{H}_0 : \chi_2^2, \end{cases} \quad (2.62)$$

where

- $\chi_2^2(\rho)$ is the noncentral chi-squared distributions with two degrees of freedom,
- χ_2^2 is the central chi-squared distributions with two degrees of freedom,
- and ρ is the noncentrality parameter, which is given by

$$\rho = \frac{|\alpha|^2}{\sigma_n^2} |\mathbf{a}^H(\theta)\mathbf{R}_x^T\mathbf{a}(\theta)|^2. \quad (2.63)$$

For the general signal model, we set δ according to a desired probability of false alarm P_{FA} , i.e.,

$$P_{\text{FA}} = P(L(\mathbf{y}) > \delta | \mathcal{H}_0) \quad (2.64)$$

$$\delta = \mathcal{F}_{\chi_2^2}^{-1}(1 - P_{\text{FA}}) \quad (2.65)$$

where $\mathcal{F}_{\chi_2^2}^{-1}$ is the inverse central chi-squared distribution function with two degrees of freedom. The probability of detection is given by

$$P_D = P(L(\mathbf{y}) > \delta | \mathcal{H}_1) \quad (2.66)$$

$$P_D = 1 - \mathcal{F}_{\chi_2^2(\rho)} \left(\mathcal{F}_{\chi_2^2}^{-1}(1 - P_{FA}) \right) \quad (2.67)$$

where $\mathcal{F}_{\chi_2^2(\rho)}$ is the noncentral chi-squared distribution function with two degrees of freedom and noncentrality parameter ρ .

2.4.3.1 P_D for Orthogonal Waveforms

For orthogonal waveforms $\mathbf{R}_x^T = \mathbf{I}_M$, therefore, the GLRT can be expressed as

$$L_{\text{Orthog}}(\hat{\theta}_{\text{ML}}) = \frac{\left| \mathbf{a}^H(\hat{\theta}_{\text{ML}}) \mathbf{E} \mathbf{a}^*(\hat{\theta}_{\text{ML}}) \right|^2}{M \mathbf{a}^H(\hat{\theta}_{\text{ML}}) \mathbf{a}(\hat{\theta}_{\text{ML}})} \underset{\mathcal{H}_0}{\overset{\mathcal{H}_1}{\gtrless}} \delta_{\text{Orthog}} \quad (2.68)$$

and the statistic of $L(\hat{\theta}_{\text{ML}})$ for this case is

$$L_{\text{Orthog}}(\hat{\theta}_{\text{ML}}) \sim \begin{cases} \mathcal{H}_1 : \chi_2^2(\rho_{\text{Orthog}}), \\ \mathcal{H}_0 : \chi_2^2, \end{cases} \quad (2.69)$$

where

$$\rho_{\text{Orthog}} = \frac{M^2 |\alpha|^2}{\sigma_n^2}. \quad (2.70)$$

We set δ_{Orthog} according to a desired probability of false alarm $P_{\text{PF-Orthog}}$, i.e.,

$$\delta_{\text{Orthog}} = \mathcal{F}_{\chi_2^2}^{-1}(1 - P_{\text{PF-Orthog}}) \quad (2.71)$$

and then the probability of detection for orthogonal waveforms is given by

$$P_{D\text{-Orthog}} = 1 - \mathcal{F}_{\chi_2^2(\rho_{\text{Orthog}})} \left(\mathcal{F}_{\chi_2^2}^{-1}(1 - P_{\text{PF-Orthog}}) \right). \quad (2.72)$$

2.4.3.2 P_D for NSP Waveforms

For spectrum sharing waveforms $\mathbf{R}_x^T = \mathbf{R}_x^T$, therefore, the GLRT can be expressed as

$$L_{\text{NSP}}(\hat{\theta}_{\text{ML}}) = \frac{\left| \mathbf{a}^H(\hat{\theta}_{\text{ML}}) \mathbf{E} \mathbf{a}^*(\hat{\theta}_{\text{ML}}) \right|^2}{M \mathbf{a}^H(\hat{\theta}_{\text{ML}}) \mathbf{R}_x^T \mathbf{a}(\hat{\theta}_{\text{ML}})} \underset{\mathcal{H}_0}{\overset{\mathcal{H}_1}{\gtrless}} \delta_{\text{NSP}} \quad (2.73)$$

and the statistic of $L(\hat{\theta}_{\text{ML}})$ for this case is

$$L_{\text{NSP}}(\hat{\theta}_{\text{ML}}) \sim \begin{cases} \mathcal{H}_1 : \chi_2^2(\rho_{\text{NSP}}), \\ \mathcal{H}_0 : \chi_2^2, \end{cases} \quad (2.74)$$

where

$$\rho_{\text{NSP}} = \frac{|\alpha|^2}{\sigma_n^2} |\mathbf{a}^H(\theta) \mathbf{R}_{\mathbf{x}}^T \mathbf{a}(\theta)|^2. \quad (2.75)$$

We set δ_{NSP} according to a desired probability of false alarm $P_{\text{PF-NSP}}$, i.e.,

$$\delta_{\text{NSP}} = \mathcal{F}_{\chi_2^2}^{-1}(1 - P_{\text{PF-NSP}}) \quad (2.76)$$

and then the probability of detection for orthogonal waveforms is given by

$$P_{\text{D-NSP}} = 1 - \mathcal{F}_{\chi_2^2(\rho_{\text{NSP}})} \left(\mathcal{F}_{\chi_2^2}^{-1}(1 - P_{\text{PF-NSP}}) \right). \quad (2.77)$$

2.4.4 Numerical Results

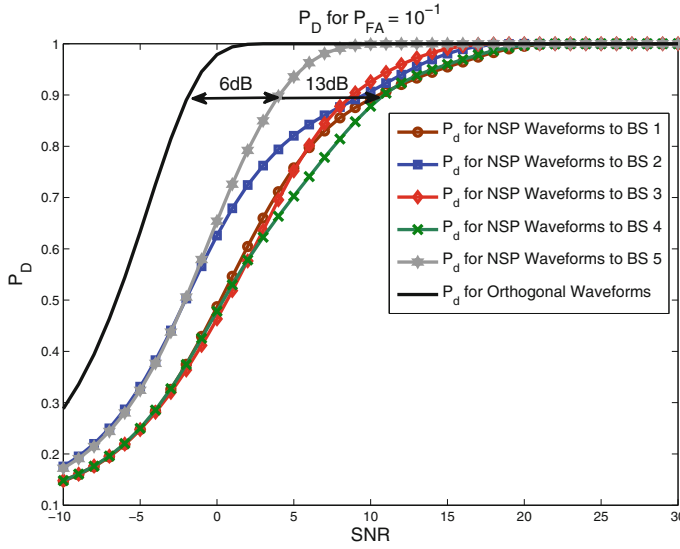
In order to study the detection performance of spectrum sharing MIMO radars, we carry out Monte Carlo simulation using the radar parameters mentioned in [19].

2.4.4.1 Analysis of Case 1

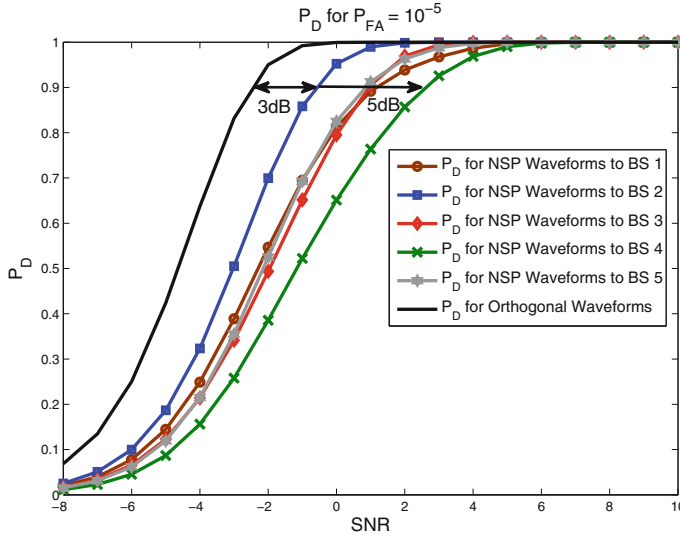
For this case, at each run of Monte Carlo simulation we generate \mathcal{K} Rayleigh interference channels each with dimensions $N^{\text{BS}} \times M$, calculate their null spaces and construct corresponding projection matrices using Algorithm 4, determine the best channel to perform projection of radar signal using Algorithm 3, transmit NSP signal, estimate parameters θ and α from the received signal, and calculate the probability of detection for orthogonal and NSP waveforms.

Performance of Algorithms 3 and 4: In Fig. 2.5, we demonstrate the use of Algorithms 3 and 4 in improving target detection performance when multiple BSs are present in detection space of radar and the radar has to reliably detect target while not interfering with communication system of interest. As an example, we consider a scenario with five BSs and the radar has to select a projection channel which minimizes degradation in its waveform, thus, maximizing its probability of detection of the target.

In Fig. 2.5a, we consider the case when $\dim \mathcal{N}(\mathbf{H}_i) = 2$. We show detection results for five different NSP signals, i.e., radar waveform projected onto five different BSs. Note that, in order to achieve a detection probability of 90%, we need 6 to 13 dB more gain in SNR as compared to the orthogonal waveform, depending upon which channel we select. Using Algorithms 3 and 4 we can select interference channel that results in minimum degradation of radar waveform and results in enhanced



(a) Probability of detection when $\dim \mathcal{N}(\mathbf{H}_i) = 2$. Note that 6 dB to 13 dB of additional gain in SNR is required to detect target with 90% probability, depending upon the NSP waveform transmitted.



(b) Probability of detection when $\dim \mathcal{N}(\mathbf{H}_i) = 6$. Note that 3 dB to 5 dB of additional gain in SNR is required to detect target with 90% probability, depending upon the NSP waveform transmitted.

Fig. 2.5 Case 1 – Performance of Algorithms 3 and 4: Using our spectrum sharing and projection algorithms, we can select interference channel for radar signal projection to maximize detection probability and minimize gain in SNR required as a result of NSP of radar waveforms. For example, Algorithms 3 and 4 select BS#5 and BS#2 for $\dim \mathcal{N}(\mathbf{H}_i) = 2$ and $\dim \mathcal{N}(\mathbf{H}_i) = 6$ cases, respectively, as they require minimum additional gain in SNR

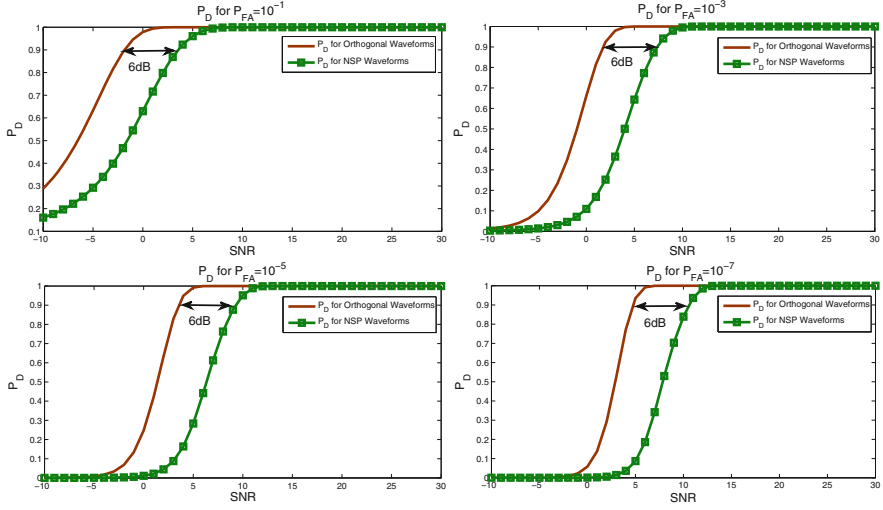


Fig. 2.6 ‘Case 1(a): $\dim \mathcal{N}(\mathbf{H}_i) = 2$ ’: P_D as a function of SNR for various values of probability of false alarm P_{FA} , i.e., $P_{FA} = 10^{-1}, 10^{-3}, 10^{-5}$ and 10^{-7} . The interference channel \mathbf{H}_i has dimensions 2×4 , i.e., the radar has $M = 4$ antennas and the communication system has $N^{BS} = 2$ antennas, thus, we have a null-space dimension of ‘ $\dim \mathcal{N}(\mathbf{H}_i) = 2$ ’. Note that we need 6 dB more gain in SNR for the NSP waveform to get the same result produced by the orthogonal waveform

target detection performance with the minimum additional gain in SNR required. For example, Algorithms 3 and 4 would select BS#5 because in this case NSP waveform requires least gain in SNR to achieve a detection probability of 90% as compared to other BSs.

In Fig. 2.5b, we consider the case when $\dim \mathcal{N}(\mathbf{H}_i) = 6$. Similar to Fig. 2.5a we show detection results for five different NSP signals but now MIMO radar has a larger array of antennas as compared to the previous case. In this case, in order to achieve a detection probability of 90%, we need 3 to 5 dB more gain in SNR as compared to the orthogonal waveform. As in the previous case, using Algorithms 3 and 4 we can select interference channel that results in minimum degradation of radar waveform and results in enhanced target detection performance with the minimum additional gain in SNR required. For example, Algorithms 3 and 4 would select BS#2 because in this case NSP waveform requires least gain in SNR to achieve a detection probability of 90% as compared to the other BSs.

The above two examples demonstrate the importance of Algorithms 3 and 4 in selecting interference channel for radar signal projection to maximize detection probability and minimize gain in SNR required as a result of NSP of radar waveforms for spectrum sharing.

Case 1(a): $\dim \mathcal{N}(\mathbf{H}_i) = 2$: In Fig. 2.6, we plot the variations of probability of detection P_D as a function of signal-to-noise ratio (SNR) for various values of probability of false alarm P_{FA} . Each subplot represents the P_D for a fixed P_{FA} . We choose to evaluate P_D against P_{FA} values of $10^{-1}, 10^{-3}, 10^{-5}$ and 10^{-7} when the interference

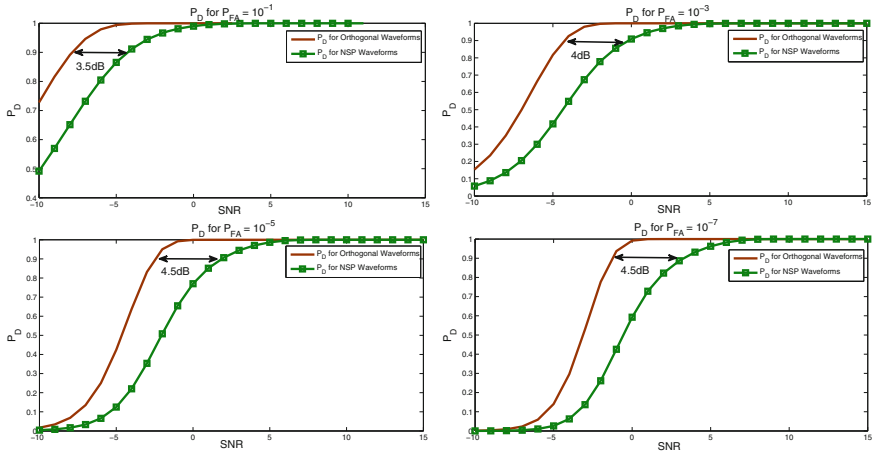


Fig. 2.7 ‘Case 1(b): $\dim \mathcal{N}(\mathbf{H}_i) = 6$ ’: P_D as a function of SNR for various values of probability of false alarm P_{FA} , i.e., $P_{FA} = 10^{-1}, 10^{-3}, 10^{-5}$ and 10^{-7} . The interference channel \mathbf{H}_i has dimensions 2×8 , i.e., the radar has $M = 8$ antennas and the communication system has $N^{BS} = 2$ antennas, thus, we have a nullspace dimension of ‘ $\dim \mathcal{N}(\mathbf{H}_i) = 6$ ’. Note that we need 3.5 to 4.5 dB more gain in SNR for the NSP waveform to get the same result produced by the orthogonal waveform

channel \mathbf{H}_i has dimensions 2×4 , i.e., the radar has $M = 4$ antennas and the communication system has $N^{BS} = 2$ antennas, thus, we have a null-space dimension of ‘ $\dim \mathcal{N}(\mathbf{H}_i) = 2$ ’. When we compare the detection performance of two waveforms we note that in order to get a desired P_D for a fixed P_{FA} we need more SNR for NSP than orthogonal waveforms. For example, say we desire $P_D = 0.9$, then according to Fig. 2.6 we need 6 dB more gain in SNR for NSP waveform to get the same result produced by the orthogonal waveform.

Case 1(b): $\dim \mathcal{N}(\mathbf{H}_i) = 6$: In Fig. 2.7, similar to Fig. 2.6, we do an analysis of P_D against the same values of P_{FA} but for interference channel \mathbf{H}_i having dimensions 2×8 , i.e., now the radar has $M = 8$ antennas and the communication system has $N^{BS} = 2$ antennas, thus, we have a null-space dimension of ‘ $\dim \mathcal{N}(\mathbf{H}_i) = 6$ ’. Similar to Case 1, when we compare the detection performance of two waveforms we note that in order to get a desired P_D for a fixed P_{FA} we need more SNR for NSP than the orthogonal waveforms. For example, say we desire $P_D = 0.9$, then according to Fig. 2.7 we need 3.5 to 4.5 dB more gain in SNR for the NSP waveform to get the same result produced by the orthogonal waveform.

Comparison of Case 1(a) and Case 1(b): As expected, when SNR increases detection performance increases for both waveforms. However, when we compare the two waveforms at a fixed value of SNR, the orthogonal waveforms perform much better than the NSP waveform in detecting target. This is because our transmitted waveforms are no longer orthogonal and we lose the advantages promised by orthogonal waveforms when used in MIMO radars as discussed in Sect. 2.1.6, but, we ensure

zero-interference to the BS of interest, thus, sharing radar spectrum at an increased cost of target detection in terms of SNR.

In Case 1(a), in order to achieve a desired P_D for a fixed P_{FA} we need more SNR for NSP as compared to Case 1(b). This is because we are using more radar antennas, while the antennas at the BS remain fixed in Case 1(b) which increases the dimension of the null space of the interference channel. This yields better detection performance even for NSP waveform. So, in order to mitigate the effect of NSP on radar performance one way is to employ a larger array at the radar transmitter.

2.4.4.2 Analysis of Case 2

For this case, at each run of Monte Carlo simulation we generate \mathcal{K} Rayleigh interference channels, combine them into one interference channel with dimensions $\mathcal{K}N^{BS} \times M$, calculate its null space and construct corresponding projection matrix using Algorithm 6, perform projection of radar signal using Algorithm 5, transmit NSP signal, estimate parameters θ and α from the received signal, and calculate the probability of detection for orthogonal and NSP waveforms.

In Fig. 2.8, we consider the case when the radar has a very large antenna array as compared to the combined antenna array of \mathcal{K} BSs. In such a scenario, we have enough degrees of freedom at the radar for reliable target detection and simultaneously nulling out interference to all the BSs present in the network. As an example, in

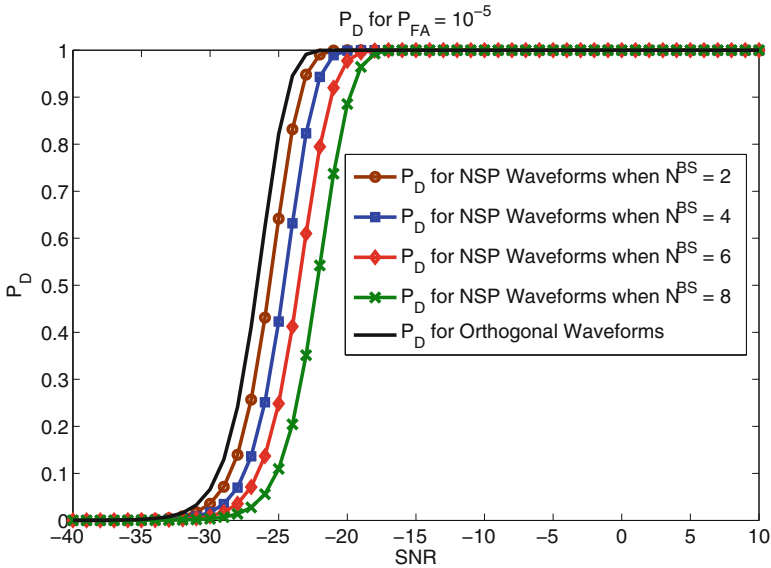


Fig. 2.8 Case 2: P_D as a function of SNR for $P_{FA} = 10^{-5}$. The MIMO radar mitigates interference to all the BSs in the network. As an example, we consider $M = 100$, $\mathcal{K} = 5$, and $N^{BS} = \{2, 4, 6, 8\}$

Fig. 2.8, we consider $M = 100$, $\mathcal{K} = 5$, and $N^{\text{BS}} = \{2, 4, 6, 8\}$. We do an analysis of P_D against $P_{\text{FA}} = 10^{-5}$ for the combined interference channel \mathbf{H} having dimensions $\mathcal{K}N^{\text{BS}} \times M$. When we compare the detection performance of original waveform and NSP waveform onto the combined channel we note that in order to get a desired P_D for a fixed P_{FA} we need more SNR for NSP than the orthogonal waveforms. For example, say we desire $P_D = 0.95$, then according to Fig. 2.8 we need 1, 2, 3.5, and 4.5 dB more gain in SNR for the NSP waveform when N^{BS} is 2, 4, 6, and 8, respectively, to get the same result produced by the orthogonal waveforms.

2.5 Conclusion

In future, radar RF spectrum will be shared with wireless communication systems to meet the growing bandwidth demands and mitigate the effects of spectrum congestion for commercial wireless services. In this chapter, we analyzed a similar spectrum sharing scenario between radars and cellular systems. We proposed a spatial approach for interference mitigation of radar signals at an LTE cellular system. We focused on a radar-centric interference-mitigation approach where our goal was to manipulate radar signals such that they were not a source of interference to a chosen LTE BS. We extended the idea to project radar signals onto the null space of interference channel for a single system to a cellular system with many base stations. We evaluated target parameter estimation and detection performance of spectrum sharing MIMO radars. We formulated the statistical detection problem for target detection and used generalized likelihood ratio test to decide about the presence of target when using orthogonal waveforms and null-space projected (NSP) waveforms. We proposed novel spectrum sharing algorithms for various cases in which MIMO radar is sharing spectrum with cellular system with minimal degradation in its performance metrics.

2.6 MATLAB Code

This section presents MATLAB code for target detection for spectrum sharing MIMO radars.

```
% Compares Pd for Multi BS side-to-side with orthogonal waveforms
% Select Mt number
% Select BS number

%% Define Parameters
% Speed of light
c = 3*10^8;
% Nr Comm Receivers
Nr=2;
% Mt Radar Transmitters
Mt=8;
% Mr Radar Receivers
```

```

Mr=Mt;
% Radial velocity of 2000 m/s
v_r = 2000;
% Radar reference point
r_0 = 500*10^3;
% Carrier frequency 3.5GHz
f_c = 3.5*10^9;
% Angular carrier frequency
omega_c=2*pi*f_c;
lambda = (2*pi*c)/omega_c;
theta=0;

%% Steering vector and Transmit Signal Correlation Matrix
% Transmit/Receive Steering vector (Mt x 1)
a = [1 exp(1i * pi * (1:Mt-1) * sin(theta))]' ;
% Transmit Correlation Matrix (Mt x Mt) for Orthonormal Waveforms
Rs = eye(Mt);

%% Define SNR for ROC (Reciever Operating Characteristics)

SNR_db=-8:1:10;
SNR_mag=10.^(SNR_db./10);
%Probability of false alarm values
P_FA = [10^-5];
%% Monte-Carlo iterations
MC_iter=10;
Pd_orthog_cell=cell(1,MC_iter);
Pd_NSP_cell=cell(1,MC_iter);
for i=1:MC_iter
%% Interference channel matrix H generation and null space computation

% Generate Cellular Channels and Find NS of them and select
% Channel with Min NS
BS =5;
% Make a cell to store matrices
BS_channels = cell(1,BS);
% Make a cell to store Projectors for every BS
Proj_matrix = cell(1,BS);
for b =1:BS
    BS_channels{b} = (randn(Nr,Mt)+1i*randn(Nr,Mt));
    Proj_matrix{b} = null(BS_channels{b}) * ...
        transpose(null(BS_channels{b}));
    Rs_null{b} = Proj_matrix{b} * Rs * Proj_matrix{b}';

% Non-centrality parameter of chi-square
for z = 1:length(SNR_mag)

    rho_orthog(b) = SNR_mag(z)*(abs(a'*Rs.'*a))^2;
    rho_NSP(b) = SNR_mag(z)*(abs(a'*Rs_null{b}.'*a))^2;

% Creates threshold values for a desired Pfa for
% an inverse central-chi-square w/ 2
% degrees of freedom

delta = chi2inv(ones(1,length(P_FA)) - P_FA, repmat(2,1,length(P_FA)));

% rows = SNR, cols = P_FA %
% ncx2cdf = Noncentral chi-square cumulative distribution function
Pd_orthog(z,:) = ones(1,length(P_FA))- ...
    ncx2cdf(delta, repmat(2,1,length(P_FA)), ...
    repmat(rho_orthog(b),1,length(P_FA)));

Pd_NSP(z,:) = ones(1,length(P_FA))- ...
    ncx2cdf(delta, repmat(2,1,length(P_FA)), ...
    repmat(rho_NSP(b),1,length(P_FA)));

end
Pd_orthog_cell{b}=Pd_orthog;

```

```

Pd_NSP_cell{b}=Pd_NSP;

end
Pd_orthog_cell_multiBS{i}=Pd_orthog_cell;
Pd_NSP_cell_multiBS{i}=Pd_NSP_cell;
Pd_orthog_cat(:, :, i) = cell2mat(Pd_orthog_cell_multiBS{i});
Pd_NSP_cat(:, :, i) = cell2mat(Pd_NSP_cell_multiBS{i});

end
Pd_orthog_cat_mean = mean(Pd_orthog_cat,3);
Pd_NSP_cat_mean = mean(Pd_NSP_cat,3);

%% Plots Probability of detection curves for given
% Probability of false alarm
figure
plot(SNR_db', Pd_NSP_cat_mean(:,1), 'g', 'LineWidth', 2.5)
hold on
plot(SNR_db', Pd_NSP_cat_mean(:,2), 'b', 'LineWidth', 2.5)

plot(SNR_db', Pd_NSP_cat_mean(:,3), 'r', 'LineWidth', 2.5)

plot(SNR_db', Pd_NSP_cat_mean(:,4), 'm', 'LineWidth', 2.5)

plot(SNR_db', Pd_NSP_cat_mean(:,5), 'y', 'LineWidth', 2.5)

plot(SNR_db', Pd_orthog_cat_mean(:,1), 'k', 'LineWidth', 2.5)

xlabel('SNR', 'fontsize', 14)
ylabel('P_D', 'fontsize', 14)
title('P_D for P_{FA} = 10^{-5}', 'fontsize', 14)
legend('P_D for NSP Waveforms to BS 1', 'P_D for NSP Waveforms to BS 2', ...
       'P_D for NSP Waveforms to BS 3', 'P_D for NSP Waveforms to BS 4', ...
       'P_D for NSP Waveforms to BS 5', 'P_D for Orthogonal Waveforms', 14)

```

References

1. A.M. Haimovich, R.S. Blum, L.J. Cimini, MIMO radar with widely separated antennas. *IEEE Signal Process. Mag.* **25**(1), 116–129 (2008)
2. J. Li, P. Stoica, MIMO radar with colocated antennas. *IEEE Signal Process. Mag.* **24**(5), 106–114 (2007)
3. M. Skolnik, *Radar Handbook*, 3rd edn. (McGraw-Hill Professional, Maidenhead, 2008)
4. J. Li, P. Stoica, *MIMO Radar Signal Processing* (Wiley-IEEE Press, New York, 2008)
5. A. Khawar, A. Abdel-Hadi, T.C. Clancy, R. McGwier, Beampattern analysis for MIMO radar and telecommunication system coexistence, in *IEEE International Conference on Computing, Networking and Communications, Signal Processing for Communications Symposium (ICNC'14 - SPC)* (2014)
6. A. Khawar, A. Abdelhadi, T.C. Clancy, Channel Modeling Between MIMO Seaborne Radar and MIMO Cellular System. (Under submission)
7. A. Khawar, A. Abdelhadi, T.C. Clancy, Performance Analysis of Coexisting Radar and Cellular System in LoS Channel. (Under submission)
8. A. Khawar, A. Abdelhadi, T.C. Clancy, 3D Channel Modeling Between Seaborne Radar and Cellular System. (Under submission)
9. A. Khawar, A. Abdel-Hadi, T.C. Clancy, On the impact of time-varying interference-channel on the spatial approach of spectrum sharing between S-band radar and communication system, in *IEEE Military Communications Conference (MILCOM)* (2014)
10. D. Tse, P. Viswanath, *Fundamentals of Wireless Communication* (Cambridge University Press, Cambridge, 2005)

11. A. Babaei, W.H. Tranter, T. Bose, A nullspace-based precoder with subspace expansion for radar/communications coexistence, in *IEEE Global Communications Conference (GLOBECOM)* (2013)
12. J.A. Mahal, A. Khawar, A. Abdelhadi, T.C. Clancy, Radar precoder design for spectral coexistence with coordinated multi-point (CoMP) system, *CoRR*, vol. abs/1503.04256, (2015)
13. Y. Noam, A. Goldsmith, Blind null-space learning for MIMO underlay cognitive radio networks,” in *Proceedings of the IEEE International Communication on Conference* (2012)
14. S. Sodagari, A. Khawar, T.C. Clancy, R. McGwier, A projection based approach for radar and telecommunication systems coexistence, in *IEEE Global Communications Conference (GLOBECOM)* (2012)
15. H. Shajaiah, A. Khawar, A. Abdel-Hadi, T.C. Clancy, Resource allocation with carrier aggregation in LTE Advanced cellular system sharing spectrum with S-band radar, in *IEEE International Symposium on Dynamic Spectrum Access Networks: SSPARC Workshop (IEEE DySPAN 2014 - SSPARC Workshop)* (McLean, USA, 2014)
16. M. Ghorbanzadeh, A. Abdelhadi, C. Clancy, A Utility Proportional Fairness Resource Allocation in Spectrally Radar-Coexistent Cellular Networks (Submitted to Milcom 2014)
17. I. Bekkerman, J. Tabrikian, Target detection and localization using mimo radars and sonars. *IEEE Trans. Signal Process.* **54**, 3873–3883 (2006)
18. S. Kay, *Fundamentals of Statistical Signal Processing: Detection Theory* (Prentice Hall, 1998)
19. A. Khawar, A. Abdelhadi, C. Clancy, Target detection performance of spectrum sharing MIMO radars. *IEEE Sens. J.* **15**, 4928–4940 (2015)

Spectrum Sharing Between Radars and Communication
Systems

A MATLAB Based Approach

Khawar, A.; Abdelhadi, A.; Clancy, T.C.

2018, XV, 102 p. 24 illus., 22 illus. in color., Softcover

ISBN: 978-3-319-56683-2